Original Article

Oxygen ultra-fine bubbles water administration prevents bone loss of glucocorticoid-induced osteoporosis in mice by suppressing osteoclasts differentiation

Takaaki Noguchi, MD[a], Kosuke Ebina, MD, PhD[a]*, Makoto Hirao, MD, PhD[a], Tokimitsu Morimoto, MD, PhD[a], Kota Koizumi, MD, PhD[a], Kazuma Kitaguchi, MD[a], Hozo Matsuoka, MD[a], Toru Iwahashi, MD[a], Hideki Yoshikawa, MD, PhD[a]

[a] *Department of Orthopaedic Surgery, Osaka University, Graduate School of Medicine, 2-2 Yamadaoka, Suita, Osaka 565-0871, Japan*

*Corresponding author:

Phone: +81 6 6879 3552; FAX: +81 6 6879 3559

E-mail address: k-ebina@umin.ac.jp (K. Ebina)

Abstract

Purpose

Ultra-fine bubbles (<200 nm in diameter) have several unique properties, and they are tested in various medical fields. The purpose of this study was to investigate the effects of oxygen ultra-fine bubbles (OUB) on glucocorticoid-induced osteoporosis (GIO) model mice.

Methods

Prednisolone (PSL, 5 mg) were subcutaneously inserted in 6-month-old male C57BL/6J mice, and 200 μl of saline, OUB diluted saline, or nitrogen ultra-fine bubbles (NUB) diluted saline was intraperitoneally injected 3 times per week for 8 weeks the day after operations. Mice were divided into 4 groups; (1) control, sham-operation + saline; (2) GIO, PSL + saline; (3) GIO+OUB, PSL + OUB-saline; (4) GIO+NUB, PSL + NUB-saline. The effects of OUB on osteoblasts and osteoclasts were examined by serially diluted OUB medium *in vitro*.

Results

Bone mass was significantly decreased in GIO [bone volume / total volume (%): control GIO: 12.6 vs. 7.9; $p<0.01$], while significantly preserved in GIO+OUB (GIO vs.

7.9 vs. 12.9; $p<0.05$). In addition, TRAP positive cells in the distal femur [mean osteoclasts number / bone surface (mm^{-1})] was significantly increased in GIO (control vs. GIO: 6.8 vs. 11.6; $p<0.01$), while suppressed in GIO+OUB (GIO vs. GIO+OUB: 11.6 vs. 7.5; $p<0.01$). NUB didn't affect these parameters. *In vitro* experiments revealed that OUB significantly inhibited osteoclastogenesis by inhibiting RANK-TRAF6-c-Fos-NFATc1 signaling, RANK-p38 MAPK signaling, and TRAP/ Cathepsin K/ DC-STAMP mRNA expression in a concentration-dependent manner. OUB didn't affect osteoblastogenesis *in vitro*.

Conclusions

OUB prevents bone loss in GIO mice by inhibiting osteoclastogenesis.

Keywords

Oxygen ultra-fine bubbles (OUB); Glucocorticoid-induced osteoporosis (GIO); Osteoclasts; Osteoblasts; c-Fos; Nuclear factor of activated T-cells 1 (NFATc1)

Mini Abstract

Oxygen ultra-fine bubbles (OUB) saline injections prevents bone loss of glucocorticoid-induced osteoporosis in mice, and OUB inhibits osteoclastogenesis via RANK-TRAF6-c-Fos-NFATc1 signaling and RANK-p38 MAPK signaling *in vitro*.

Introduction

Ultra-fine bubbles (UFB), also referred to as nanobubbles, are miniature gas bubble in liquids with <200 nm in diameter, and possess many unique physical properties [1, 2]. UFB remains stable in liquids for long periods at a high concentration owing to their negatively charged surface and high internal pressure, whereas macrobubbles (>50 μm in diameter) increase in size and rapidly burst at a liquids surface [3, 4]. Previous reports have demonstrated that UFB increase the oxygen pressure in liquids to a greater extent than that of microbubbles (10–50 μm in diameter) [1, 4], and the high oxygen gas solubility of UFB can be beneficial for oxygenation of hypoxic tissues [5-7]. Nano-technologies are gaining a lot of recognition in the medical field, and its usefulness for ultrasound imaging and drug delivery have been demonstrated [8]. Moreover, we have previously demonstrated that the administration of oxygen ultra-fine bubbles (OUB) and air ultra-fine bubbles (AUB) promote the growth of plant, animal and fish [2], and oral administration of OUB water

reduced calcium oxalate deposits in rat kidney [9], indicating its usefulness for clinical applications. However, no reports have assessed the effects of OUB on bone metabolism.

Local oxygen concentration is strongly associated with bone metabolism. For example, hyperoxia inhibits osteoclasts differentiation [10], and promotes osteoblasts differentiation [11, 12], whereas hypoxia promotes osteoclasts differentiation [12, 13]. Indeed, it has been reported that partial pressure of oxygen (PO_2) in arterial blood is about 12%, whereas that in venous blood is about 5% [11] and in human bone was about 6.6% [14], suggesting hypoxic condition in bone. Moreover, a previous report has suggested that PO_2 in environments such as the poorly vascularized bone marrow of the elderly or glucocorticoid-induced osteoporosis (GIO) may be considerably lowered [15]. Taken together, we hypothesized that OUB administration may improve local hypoxic condition, and may have beneficial effects on bone metabolism.

Glucocorticoids are widely used to treat various immune-mediated diseases, such as patients with rheumatic diseases, who tend to be prescribed for long duration [16, 17]. GIO is a clinically serious long-term side effect of glucocorticoid treatment which affects 0.5% of the general population [18, 19], and 30-50% of patients with chronic glucocorticoid therapy suffers osteoporotic fracture [20]. The most common anti-osteoporotic agents used in the treatment of GIO are bisphosphonates (BP) [21], while it remains unclear that

whether prolonged BP treatment for GIO and postmenopausal osteoporosis are associated with similar safety issues [17], and patients treated with BP and glucocorticoid are at the higher risk of osteonecrosis of the jaw [22]. Therefore, some alternative treatment options may be required. In this study, we assessed the effects of OUB administration in GIO model mice, and demonstrated the effects of OUB on bone metabolism for the first time.

Materials and methods

UFB diluted saline and medium preparation

At first, fine microbubbles of gas were generated with brief sonication of liquid (saline or culture medium) and gas (oxygen or nitrogen) by microbubble generator. Then, these microbubbles, liquid, and gas were put into an ultra-fine bubble aerator (BUVITAS; Ligaric Company Limited, Osaka, Japan), gas-liquid mixing system which high-speed centrifugal force separates the microbubbles into UFB by the strong shearing force as previously described [2] (Fig. 1a). Nitrogen was selected as a negative control as it is abundantly contained in the atmosphere. Dissolved oxygen concentrations of OUB and nitrogen ultra-fine bubbles (NUB) diluted saline or medium were measured at 30 minutes after generation by Winkler's method as previously described [2] (Fig. 1b). UFB diluted liquid was filtered immediately after generation, using a 220 nm pore size cellulose acetate

membrane (Corning, New York, USA) to avoid contamination. This UFB saturated liquid is considered as 100%, and gradually diluted immediately before the experiment by the same non-UFB liquid to 75, 50, and 25%, respectively. In addition, we have previously described that size, concentration, and dissolved oxygen concentration of OUB produced by this methods were stable in liquid up to day 70 in 4°C [2], so OUB diluted liquid was kept in 4°C with the tight lid, and re-generated every 2 months. To confirm the concentration and size of nanoparticles, saline, OUB diluted saline, saline-injected mice serum, and OUB saline-injected mice serum were measured by NanoSight NS 300 (NanoSight Ltd, Salisbury, UK) (Supplemental material and methods) [2]. To confirm the contamination of metal nanoparticles by UFB generation, chemical analysis of both raw water and air UFB diluted water was performed by using NexION 350D ICP-MS spectrometer (PerkinElmer Inc., Shelton, USA). (Supplemental material and methods).

Mice

Six-month-old male C57BL/6J mice were purchased from Charles River Laboratories (Osaka, Japan). Pellets of PSL (5 mg) (Innovative Research of America, Sarasota, Florida, USA) were inserted subcutaneously in the nape of the neck as previously described [23], and 200 µl of saline, OUB diluted saline or NUB diluted saline was administered by

intraperitoneal injection 3 times per week for 8 weeks from the next day of operations (Fig. 1c). Mice were divided into four groups: (1) control, sham-operation + saline injections (n=8); (2) GIO, PSL pellets + saline injections (n=8); (3) GIO+OUB, PSL pellets + OUB-saline injections (n=11); and (4) GIO+NUB, PSL pellets + NUB-saline injections (n=8). All mice were housed in a temperature- and humidity-controlled facility with a 12 hour light/dark cycle and had free access to standard chow and water for 8 weeks before being euthanized. Mice were anaesthetized with an intraperitoneal injection of 0.3 mg/kg medetomidine, 4.0 mg/kg midazolam, and 5.0 mg/kg butorphanol when they were euthanized to collect bone and serum samples [24]. The serum concentration of cross linked C terminal telopeptides of type I collagen (CTX-1) (CUSABIO, Hubei, China) and osteocalcin (Takara Bio, Shiga, Japan) were measured by ELISA kit according to the manufacturer's protocol. All experimental protocols were approved by the Ethics Review Committee for Animal Experimentation of Osaka University Graduate School of Medicine (permission number: 24-022-007).

Micro-computed tomography (micro-CT) scan

The distal femurs of mice (500 μm above the growth plate) were evaluated by micro-CT (Rigaku Mechatronics, Tokyo, Japan). The results were analyzed by Tri/3D Bon software

(Ratoc System Engineering Co., Ltd., Tokyo, Japan) for parameters including bone volume fraction (BV/TV: bone volume/total volume), trabecular number (TbN), cortical bone ratio (Cv/Av: cortical volume / all volume), and mean cortical bone thickness as previously described [25].

Histology

After micro-CT scanning, bone specimens were fixed in 10% neutral-buffered and decalcified for embedding. Histological sections were stained with TRAP (Cosmo bio, Tokyo, Japan) according to the manufacturer's protocol. TRAP-positive osteoclasts were counted as previously described [26].

Cell culture

Murine primary osteoclasts were obtained from bone marrow (BM) cells flushed from the femurs and tibiae of C57BL/6J mice. These cells were cultured in α-minimum essential medium (α-MEM) containing 10% fetal bovine serum (FBS) (Equitech-Bio, Kerrville, TX, USA) and 1% penicillin and streptomycin with 5 ng/ml macrophage colony-stimulating factor (M-CSF) (R&D Systems, Minneapolis, Minnesota, USA) overnight at 37°C under

20% O_2 condition as previously described [27]. Non-adherent cells were washed twice with phosphate buffered saline (PBS) (pH=7.4) and adherent cells were seeded in 12-well plates and 48-well plates at 1×10^6 cells per well in an OUB diluted medium (concentration: 0, 25, 50, 75 and 100%) stimulated with 10 ng/ml M-CSF and 50 ng/ml receptor activator of nuclear factor kappa B ligand (RANKL) (R&D Systems) simultaneously to induce osteoclastogenesis for 5 days under 5% or 20% O_2 condition.

Murine primary osteoblasts were isolated from the calvaria of 3-day-old C57BL/6J mice (Charles River Laboratories) by sequential collagenase digestion and MC3T3-E1 cells of osteoblastic cell linage were purchased from Riken Cell Bank (Tsukuba, Japan). These cells were cultured in α-MEM containing 10% FBS and 1% penicillin and streptomycin at 37°C under 20% O_2 condition as previously described [28]. Cells were cultured in 12-well plates and 24-well plates at 1×10^5 cells per well in an OUB diluted medium (concentration: 0, 25, 50, 75 and 100%) for 5 days under 20% O_2 condition. Media were changed to osteoblasts differentiation induction medium containing 10 mM β-glycerophosphate (Calbiochem, San Diego, CA, USA) and 50 μg/ml ascorbic acid (Sigma-Aldrich, St. Louis, MO, USA) after the cells reached 60-70% confluence under 20% O_2 condition.

Osteoclastic cells derived human peripheral blood mononuclear cells (PBMC)

PBMC were extracted from human blood using Ficoll-Paque (GE Healthcare UK Ltd., Buckinghamshire, UK) according to the manufacturer's protocol. Then, CD14-positive cells were subsequently isolated from these PBMC by positive selection with anti-CD14-coated microbeads (Miltenyi Biotec, Bergisch, Gladbach, Germany) in a SuperMACS (Miltenyi Biotec) according to the manufacturer's instructions. These CD14-positive cells were cultured with 10 ng/ml M-CSF and 50 ng/ml RANKL simultaneously to induce osteoclastogenesis for 7 days under 20% O_2 condition in an OUB diluted medium (concentration: 0, 25, 50, 75 and 100%).

TRAP-staining

Osteoclastic cells from mouse BM were incubated for 5 days under 5% or 20% O_2 condition and those from human PBMC were incubated for 7 days under 20% O_2 condition in an OUB diluted medium (concentration: 0, 25, 50, 75 and 100%) using 48-well plates. At the end of the incubation period, cells were fixed with 10% formalin and washed with PBS. TRAP-staining was performed using a TRAP-staining kit (Cosmo Bio) according to the manufacturer's protocol. The total number of TRAP-positive cells with 3 or more nuclei were counted for quantification in a well and the morphology of osteoclasts was photographed as previously described [29].

Resorption pit assay

Osteoclastic cells from mouse BM were incubated for 5 days and those from human PBMC were incubated for 7 days under 20% O_2 condition in an OUB diluted medium (concentration: 0, 25, 50, 75 and 100%) using Osteo-Assay Surface 96 Well Multiple Well Plates (Corning). To analyze the surface of wells for pit formation, the medium was aspirated from the wells, and 100 µl of 10% bleach solution (6% NaOCl) was added. Cells were incubated with the bleach solution for 5 minutes at room temperature. The wells were washed twice with distilled water and allowed to dry at room temperature for 3 to 5 hours. Individual pits, or multiple pit clusters, were observed using a microscope at 200x magnification.

Western blotting (WB)

Cells were homogenized with 100 µl of radio-immunoprecipitation assay (RIPA) buffer (Pierce, Rockford, IL, USA), and complete cell lysis was obtained using a sonicator for 7.5 minutes. The lysates were centrifuged at 12,000 rpm for 5 minutes at 4°C to remove debris and the supernatants were used for electrophoresis after a protein assay using a

bicinchoninic acid (BCA) assay kit (Pierce) and transferred to a polyvinylidene difluoride (PVDF) membrane (Nippon Genetics, Tokyo, Japan) as previously described [30]. WB was performed using the following antibodies purchased from Cell Signaling Technology (Danvers, MA, USA): anti-c-Fos antibody (1:1000), anti-nuclear factor of activated T-cells 1 (NFATc1) antibody (1:1000), phosphate anti-extracellular signal-regulated kinase 1/2 (ERK1/2) antibody (Thr202/Tyr204) (1:2000), anti-ERK1/2 antibody (p44/42) (1:1000), phosphate anti-p38 antibody (Thr180/Tyr182) (1:1000), anti-p38 antibody (1:1000), phosphate anti-nuclear factor-kappa B (NF-κB) p65 antibody (Ser536) (1:1000), anti-NF-κB p65 antibody (1:1000), anti-hypoxia-inducible factor 1α (HIF1α) antibody (D2U3T) (1:1000), and anti-β-actin antibody (1:2000).

Extraction of the RNA from cultured cells, and first-strand complementary DNA (cDNA) synthesis

Total RNA was extracted from cells in 12-well plate using a RNAeasy Mini Kit (Qiagen, Düsseldorf, Germany) according to the manufacturer's protocol, and first-strand cDNA was reverse-transcribed from total RNA (1 μg) using the SuperScriptⅢ First-Strand Synthesis System (Life Technologies, Tokyo, Japan) according to the manufacturer's protocol.

Quantitative real-time polymerase chain reaction (PCR)

Real-time PCR was performed using the Step One Plus Real-Time PCR System (Life Technologies). Each cDNA sample was evaluated using a Fast SYBR Green Master Mix (Life Technologies) and expression values were normalized to hypoxanthine phosphoribosyltransferase 1 (HPRT1). PCR primers (forward and reverse, respectively) were as follows: HPRT1 (5'-CTGGTGAAAAGGACCTCTCGAA-3' and 5'-CTGAAGTACTCATTATAGTCAAGGGCAT-3'), tumor necrosis factor receptor associated factor 6 (TRAF6) (5'-AGCCCACGAAAGCCAGAAGAA-3' and 5'-CCCTTATGGATTTGATGATGC-3'), c-Fos (5'-AAACCGCATGGAGTGTGTTGTTCC-3' and 5'-TCAGACCACCTCGACAATGCATGA-3'), NFATc1 (5'-CCGTTGCTTCCAGAAAATAACA-3' and 5'-TGTGGGATGTGAACTCGGAA-3'), TRAP (5'-GGGACAATTTCTACTTCACTGGAG-3' and 5'-TCAGAGAACACGTCCTCAAAGG-3'), dendritic cell-specific transmembrane protein (DC-STAMP) (5'-GACCTTGGGCACCAGTATTT-3' and 5'-CAAAGCAACAGACTCCCAAA-3'), Cathepsin K (5'-CCATATGTGGGCCCAGGATG-3' and 5'-TCAGGGCTTTCTCGTTCCC-3'),

nuclear factor kappa B (RANK) (5'-AGAAGACGGTGCTGGAGTCT-3' and 5'-TAGGAGCAGTGAACCAGTCG-3'), HIF1α (5'-TGGCTCCCTATATCCCAATG-3' and 5'-GGTCTGCTGGAACCCAGTAA-3'), alkaline phosphatase (ALP) (5'-AATCGGAACAACCTGACTGACC-3' and 5'-TCCTTCCACCAGCAAGAAGAA-3'), Osteocalcin (5'-CTCACTCTGCTGGCCCTG-3' and 5'-CCGTAGATGCGTTTGTAGGC-3'), RANKL (5'-TGGAAGGCTCATGGTTGGAT-3' and 5'-CATTGATGGTGAGGTGTGCAA-3'), and Osteoprotegerin (OPG) (5'-ACCCAGAAACTGGTCATCAGC-3' and 5'-CTGCAATACACACACTCATCACT-3').

ALP staining and ALP activity assay

Osteoblastic cells were incubated for 5 days in an OUB diluted medium (concentration: 0, 25, 50, 75 and 100%) under 20% O_2 condition. For ALP staining, cells were washed once with PBS after fixation with 10% formalin and stained using ALP substrate solution 0.1 mg/ml naphthol AS-MX (Sigma-Aldrich), and 0.6 mg/ml fast violet B salt (Sigma-Aldrich) in 0.1 M Tris-HCl for 20 minutes. For the ALP activity assay, cells were washed twice with PBS and lysed with mammalian protein extraction reagent (MPER)

(Pierce) according to the manufacturer's protocol. ALP activity was measured using a Lab Assay ALP activity kit (Wako Pure Chemical Industries, Ltd., Japan) and protein was quantified using the Bicinchoninic Acid Protein Assay Kit (Pierce).

Statistical analysis

All data are expressed as the mean ± standard deviation (SD). Differences between the groups were assessed using the Mann-Whitney U-test. A probability value of <0.05 was considered to indicate statistical significance.

Results

Dissolved oxygen concentrations of OUB and NUB diluted saline and medium immediate after the generation

OUB significantly increased oxygen concentration of both saline (non-UFB vs. OUB: 8.3 vs. 18.0 mg/L; $p<0.01$) and medium (non-UFB vs. OUB: 9.0 vs. 17.2 mg/L; $p<0.01$), while NUB significantly decreased oxygen concentration of both saline (non-UFB vs. NUB: 8.3 vs. 2.7 mg/L; $p<0.05$) and medium (non-UFB vs. NUB: 9.0 vs. 3.1 mg/L; $p<0.05$) (Fig. 1b).

Increased nanoparticles in OUB diluted saline and OUB diluted saline injected mice serum

None of nanoparticles were detected in normal saline, although abundant nanoparticles were detected in OUB diluted saline (supplemental Fig. 1a). On the other hand, saline injected serum showed abundant total number (4.3×10^{12} particles/ml) and peak number (2.0×10^{11} particles/ml in 45nm size) of nanoparticles, in accordance with the results of previous report demonstrating the presence of serum-derived nanoparticles in mammalian [31]. Finally, OUB-saline injected serum showed higher total number (5.6×10^{12} particles/ml), peak number (2.9×10^{11} particles/ml in 50nm size), and Brownian motion of nanoparticles compared to saline injected serum (supplemental Fig. 1b, 1c, and 1d), suggesting that intraperitoneally injected OUB increased serum nanoparticles number.

Detection of metal nanoparticles in raw water and air UFB diluted water

As shown in supplemental Fig. 2, no apparent difference was observed in metal nanoparticles concentration between raw water and air UFB diluted water, suggesting little effect of UFB generation on metal nanoparticles contamination.

Effects of OUB on bone mass in GIO mice

Trabecular and cortical bone of distal femurs were assessed by micro-CT (Fig. 2a). BV/TV and TbN of trabecular bone was significantly decreased in GIO mice compared to control mice [BV/TV (%): control vs. GIO: 12.6 vs. 7.9; $p<0.01$ / TbN (1/mm): control vs. GIO: 3.6 vs. 2.5; $p<0.01$]. OUB treatment prevented these BV/TV loss (GIO vs. GIO+OUB: 7.9 vs. 12.9; $p<0.05$) and TbN loss (GIO vs. GIO+OUB: 2.5 vs. 3.4; $p<0.05$), although NUB treatment had no significant effects (Fig. 2b). Cv/Av was significantly decreased in GIO mice as compared to control mice (control vs. GIO: 36.7 vs. 32.8; $p<0.05$), while OUB treatment prevented this cortical bone loss (GIO vs. GIO+OUB: 32.8 vs. 35.7; $p<0.05$) but NUB treatment showed no significant effects as compared to GIO group (Fig. 2c). Same tendency was observed in mean cortical bone thickness, while didn't reached significant difference (Fig. 2c).

Effects of OUB on osteoclasts number and bone turnover markers in vivo

TRAP-staining of distal femurs revealed that number of osteoclasts in trabecular bone was significantly increased in GIO mice as compared to control mice (control vs. GIO: 6.8 vs.

11.6 mm^{-1}; $p<0.01$), while significantly decreased by OUB treatment (GIO vs. GIO+OUB: 11.6 vs. 7.5 mm^{-1}; $p<0.01$) but not by NUB treatment (GIO vs. GIO+NUB: 11.6 vs. 12.2 mm^{-1}; $p=0.39$) (Fig. 2d, e). The same patterns observed in trabeculae via histology were observed in cortical bone and were consistent with the micro-CT data (Fig. 2d). The ELISA of serum bone turnover markers revealed that the bone resorption marker CTX-1 was significantly increased in GIO group (control vs. GIO: 4.2 vs. 5.4 ng/ml; $p<0.05$), while significantly decreased by OUB treatment (GIO vs. GIO+OUB: 5.4 vs. 4.5 ng/ml; $p<0.05$). In contrast, the bone formation marker osteocalcin was significantly decreased in GIO group (control vs. GIO: 33.8 vs. 24.8 ng/ml; $p<0.05$), while showed not significant response to OUB treatment (GIO vs. GIO+OUB: 24.8 vs. 28.6 ng/ml; $p=0.52$) (Fig. 2f).

Effects of OUB on osteoclastogenesis in mouse BM cells under 5% or 20% O_2 condition in vitro

The effects of OUB on osteoclastogenesis in mice were evaluated in an OUB diluted medium under 20% O_2 condition. OUB significantly decreased the number of TRAP-positive cells in a dose dependent manner (Fig. 3a). In addition, OUB significantly inhibited the bone resorption activity of osteoclasts in a dose dependent manner (Fig. 3b). As for cell-signaling, WB revealed that OUB down-regulated the c-Fos and NFATc1

proteins, and the phosphorylation of p38 in a dose dependent manner (Fig. 3c). Real-time PCR analysis showed that OUB significantly inhibited osteoclast-related mRNA (TRAF6, c-Fos, NFATc1, TRAP, Cathepsin K, DC-STAMP) expression in a dose dependent manner, while didn't affect the mRNA levels of RANK and HIF1α (Fig. 3d). A schematic diagram of the signaling pathways involved in osteoclasts differentiation treated with OUB is shown in Fig. 5c.

The effects of OUB on osteoclastogenesis in mice were evaluated in OUB diluted medium under 5% O_2 condition, mimicking hypoxia of bone marrow. OUB significantly decreased the number of TRAP-positive cells in a dose dependent manner (Fig. 4a). Western blotting revealed that protein levels of HIF1α was promoted by hypoxia (5% O_2) compared to normoxia (20% O_2), although no apparent difference was observed between 0% and 100% OUB treated osteoclasts (Fig. 4b). Real-time PCR analysis showed that OUB significantly inhibited osteoclast-related mRNA (TRAF6, c-Fos, NFATc1, TRAP, Cathepsin K, DC-STAMP) expression in a dose dependent manner, while didn't affect the mRNA levels of HIF1α (Fig. 4c).

Effects of OUB on osteoclastogenesis in human PBMC under 20% O_2 condition in vitro

The effects of OUB on osteoclastogenesis in human PBMC were also evaluated. OUB significantly decreased the number of TRAP-positive cells (Fig. 5a) and the bone resorption activity (Fig. 5b) in a dose dependent manner, similar to the results we report in mice.

Effects of OUB on osteoblastogenesis in mouse calvarial cells and MC3T3-E1 cells under 20% O_2 condition

The effects of OUB on osteoblasts differentiation were investigated using OUB diluted medium (concentration: 0, 25, 50, 75 and 100%). OUB administration didn't affect ALP activity and ALP staining in mouse calvarial cells and MC3T3-E1 cells (Fig. 6a). In addition, OUB didn't significantly affect the mRNA expression of ALP, osteocalcin, RANKL, OPG and HIF1α in mouse calvarial cells (Fig. 6b).

Discussion

To the best of our knowledge, this is the first report demonstrating the effect of OUB on bone metabolism, and our results revealed that OUB preserved bone loss in GIO mice.

Important roles of oxygen tension on bone metabolism has been reported. Concerning osteoclastogenesis, previous reports have shown that hypoxia (1-2% PO_2) stimulates osteoclasts formation [13], whereas hyperoxia (95% PO_2) suppresses osteoclasts formation and bone resorption through the reduction of RANK, NFATc1, and DC-STAMP expression [10]. Alternatively, hypoxia (0.2% PO_2) inhibits differentiation of rat osteoblasts [11].

A previous report has demonstrated that saline solution containing oxygen microbubbles (<50 μm in diameter) improved a hypoxic condition in blood in a dose dependent manner, suggesting that oxygen microbubbles may be a potentially effective tool for the oxygenation of hypoxic tissue [4]. In addition, the clinical application of microbubbles and nanobubbles have been reported. Drugs encapsulated in microbubbles can be focally released at a targeted tissue and incorporated by various cells [32-36], and the oral intake of OUB-containing water reduced expression of monocyte chemoattractantprotein-1 in the kidneys of ethylene glycol-treated rats [9]. Taken together, OUB may affect target cells *in vivo* and *in vitro*, and we hypothesized that OUB administration may be effective at improving a hypoxic condition and preserving bone loss in GIO mice.

Concerning osteoclastogenesis signaling, RANKL binds to its membrane bound receptor RANK on monocytic precursors, and RANKL-induced osteoclasts formation is transduced

by TRAF6 ubiquitination, and following nuclear translocations of NF-κB, AP-1 (c-Fos/c-Jun dimer) and NFATc1 [37]. Downregulation of TRAF6 lead to decreased TRAF6 ubiquitination and osteoclasts formation [37]. On the other hand, hypoxia (2% PO_2) increased HIF1α activity and expression [38], and consequent osteoclasts formation [39]. In this study, OUB down-regulated the expression of TRAF6, c-Fos and NFATc1, and phosphorylation of p38, although RANK, HIF1α, ERK1/2, and NF-κB expression and phosphorylation in osteoclasts were unaffected. Taken together, OUB may attenuate RANK-TRAF6-c-Fos-NFATc1 signaling and RANK-p38 MAPK signaling, without altering elements related to oxygen-concentration such as RANK, HIF1α, ERK1/2, and NF-κB [10, 40, 41] (Fig. 5C).

On the other hand, OUB didn't significantly affect osteoblasts differentiation. A previous report has demonstrated that hypoxia (2% O_2) decreased mineralization as compared to normoxia (20% O_2) [42], although intensive hyperoxia (90% O_2) increased ALP activity and the collagen synthesis of osteoblasts [43]. We have previously reported that the increase of oxygen concentration in water containing OUB at 70 days after generation was relatively small compared to normal water (approximately 9.2 vs. 7.8 mg/L) [2], and PO_2 of swine venous blood increased from 64.6 mmHg to 81.9 mmHg in a 10% oxygen microbubbles dilution [4]. There are no other reports demonstrating the effect of this "mild

hyperoxia" on bone metabolism, and oxygen-related gene expression may not be influenced in this situation and time course.

There are several limitations in this study. First, the size of UFB is so small that it is technically difficult to detect its bioavailability in the circulation. Second, there may be differences in the response to OUB between cells types such as osteoclasts and osteoblasts, although the precise mechanisms of how OUB affect cell signaling (receptor, endocytosis, etc.) remain to be elucidated. Third, our preliminary experiments using high-concentration NUB diluted medium showed some apoptosis of cultured cells which was never seen in OUB experiments, and was difficult to assess the effects of NUB *in vitro*. Taken together, the effects of OUB on osteoclasts may be exerted by oxygen at least in part, but not only by UFB itself. Further interest is that OUB may be more effective under conditions of high bone turnover such as postmenopausal osteoporosis, and for convenient clinical application, effects of OUB by oral administration or combination with other anti-osteoporosis agents may be confirmed in future studies.

In conclusion, OUB prevents bone loss associated with GIO in mice by inhibiting osteoclastogenesis via RANK-TRAF6-c-Fos-NFATc1 signaling and RANK-p38 MAPK signaling, indicating OUB as a hopeful treatment option for GIO.

Acknowledgments

We are grateful to M. Shinkawa and A. Tada for excellent technical assistance. We thank all the members of Yoshikawa's laboratory for the helpful discussion and comments.

Authors' roles

Study design: TN, KE, MH and HY. Study conduct: TN and KE. Data collection: TN, KE, MH, TM, KK, KK, HM and TI. Data analysis: TN and KE. Data interpretation: TN, KE and MH. Drafting the manuscript: TN and KE. Approving the final version of manuscript: TN, KE, MH, TM, KK, KK, HM, TI and HY. KE takes responsibility for the integrity of the data analysis.

Conflicts of interest

All oxygen and nitrogen ultra-fine bubbles diluted saline and medium were prepared by Ligaric Company Limited. This research was funded by Nakatomi funding, Health and Labor Sciences Research Grant of Japan, Ligaric Company Limited, and West Nippon Expressway Company. The funders had no role in the study design, decision to publish, or preparation of the manuscript.

References

1. Agarwal A, Ng WJ, Liu Y (2011) Principle and applications of microbubble and nanobubble technology for water treatment. Chemosphere 84:1175-1180

2. Ebina K, Shi K, Hirao M, Hashimoto J, Kawato Y, Kaneshiro S, Morimoto T, Koizumi K, Yoshikawa H (2013) Oxygen and air nanobubble water solution promote the growth of plants, fishes, and mice. PloS one 8:e65339

3. Takahashi M, Chiba K, Li P (2007) Free-radical generation from collapsing microbubbles in the absence of a dynamic stimulus. The journal of physical chemistry B 111:1343-1347

4. Matsuki N, Ichiba S, Ishikawa T, Nagano O, Takeda M, Ujike Y, Yamaguchi T (2012) Blood oxygenation using microbubble suspensions. European biophysics journal : EBJ 41:571-578

5. Bitterman H (2009) Bench-to-bedside review: oxygen as a drug. Critical care 13:205

6. Abdelsalam M, Cheifetz IM (2010) Goal-directed therapy for severely hypoxic patients with acute respiratory distress syndrome: permissive hypoxemia. Respiratory care 55:1483-1490

7. Guo S, Dipietro LA (2010) Factors affecting wound healing. Journal of dental research 89:219-229

8. Wang Y, Li X, Zhou Y, Huang P, Xu Y (2010) Preparation of nanobubbles for ultrasound imaging and intracelluar drug delivery. International journal of pharmaceutics 384:148-153

9. Hirose Y, Yasui T, Taguchi K, et al. (2013) Oxygen nano-bubble water reduces calcium oxalate deposits and tubular cell injury in ethylene glycol-treated rat kidney. Urolithiasis 41:279-294

10. Al Hadi H, Smerdon GR, Fox SW (2013) Hyperbaric oxygen therapy suppresses osteoclast formation and bone resorption. Journal of orthopaedic research : official publication of the Orthopaedic Research Society 31:1839-1844

11. Utting JC, Robins SP, Brandao-Burch A, Orriss IR, Behar J, Arnett TR (2006) Hypoxia inhibits the growth, differentiation and bone-forming capacity of rat osteoblasts. Experimental cell research 312:1693-1702

12. Arnett TR (2010) Acidosis, hypoxia and bone. Archives of biochemistry and biophysics 503:103-109

13. Utting JC, Flanagan AM, Brandao-Burch A, Orriss IR, Arnett TR (2010) Hypoxia stimulates osteoclast formation from human peripheral blood. Cell biochemistry and function 28:374-380

14. Harrison JS, Rameshwar P, Chang V, Bandari P (2002) Oxygen saturation in the bone marrow of healthy volunteers. Blood 99:394

15. Lewis JS, Lee JA, Underwood JC, Harris AL, Lewis CE (1999) Macrophage responses to hypoxia: relevance to disease mechanisms. Journal of leukocyte biology 66:889-900

16. Van Staa TP, Laan RF, Barton IP, Cohen S, Reid DM, Cooper C (2003) Bone density threshold and other predictors of vertebral fracture in patients receiving oral glucocorticoid therapy. Arthritis and rheumatism 48:3224-3229

17. Rizzoli R, Adachi JD, Cooper C, et al. (2012) Management of glucocorticoid-induced osteoporosis. Calcified tissue international 91:225-243

18. van Staa TP, Leufkens HG, Cooper C (2002) The epidemiology of corticosteroid-induced osteoporosis: a meta-analysis. Osteoporosis international : a journal established as result of cooperation between the European Foundation for Osteoporosis and the National Osteoporosis Foundation of the USA 13:777-787

19. Toth M, Grossman A (2013) Glucocorticoid-induced osteoporosis: lessons from Cushing's syndrome. Clinical endocrinology 79:1-11

20. Mazziotti G, Angeli A, Bilezikian JP, Canalis E, Giustina A (2006) Glucocorticoid-induced osteoporosis: an update. Trends in endocrinology and metabolism: TEM 17:144-149

21. Suzuki Y, Nawata H, Soen S, et al. (2014) Guidelines on the management and treatment of glucocorticoid-induced osteoporosis of the Japanese Society for Bone and Mineral Research: 2014 update. Journal of bone and mineral metabolism 32:337-350

22. Khan AA, Morrison A, Hanley DA, et al. (2015) Diagnosis and management of osteonecrosis of the jaw: a systematic review and international consensus. Journal of bone and

mineral research : the official journal of the American Society for Bone and Mineral Research 30:3-23

23. Yoon HY, Won YY, Chung YS (2012) Poncirin prevents bone loss in glucocorticoid-induced osteoporosis in vivo and in vitro. Journal of bone and mineral metabolism 30:509-516

24. Kawai S, Takagi Y, Kaneko S, Kurosawa T (2011) Effect of three types of mixed anesthetic agents alternate to ketamine in mice. Experimental animals / Japanese Association for Laboratory Animal Science 60:481-487

25. Noguchi T, Ebina K, Hirao M, et al. (2015) Progranulin plays crucial roles in preserving bone mass by inhibiting TNF-alpha-induced osteoclastogenesis and promoting osteoblastic differentiation in mice. Biochemical and biophysical research communications 465:638-643

26. He Y, Rhodes SD, Chen S, et al. (2012) c-Fms signaling mediates neurofibromatosis Type-1 osteoclast gain-in-functions. PloS one 7:e46900

27. Hu M, Bassett JH, Danks L, et al. (2011) Activated invariant NKT cells regulate osteoclast development and function. Journal of immunology 186:2910-2917

28. Schmidt K, Schinke T, Haberland M, Priemel M, Schilling AF, Mueldner C, Rueger JM, Sock E, Wegner M, Amling M (2005) The high mobility group transcription factor Sox8 is a negative regulator of osteoblast differentiation. The Journal of cell biology 168:899-910

29. Ritchlin CT, Haas-Smith SA, Li P, Hicks DG, Schwarz EM (2003) Mechanisms of TNF-alpha- and RANKL-mediated osteoclastogenesis and bone resorption in psoriatic arthritis. The Journal of clinical investigation 111:821-831

30. Imura Y, Yasui H, Outani H, et al. (2014) Combined targeting of mTOR and c-MET signaling pathways for effective management of epithelioid sarcoma. Molecular cancer 13:185

31. Peng HH, Martel J, Lee YH, Ojcius DM, Young JD (2011) Serum-derived nanoparticles: de novo generation and growth in vitro, and internalization by mammalian cells in culture. Nanomedicine (Lond) 6:643-658

32. Xie X, Lin W, Liu H, Deng J, Chen Y, Liu H, Fu X, Yang Y (2015) Ultrasound-responsive nanobubbles contained with peptide-camptothecin conjugates for targeted drug delivery. Drug delivery 1-9

33. Huang HY, Liu HL, Hsu PH, Chiang CS, Tsai CH, Chi HS, Chen SY, Chen YY (2015) A multitheragnostic nanobubble system to induce blood-brain barrier disruption with magnetically guided focused ultrasound. Advanced materials 27:655-661

34. Geis NA, Katus HA, Bekeredjian R (2012) Microbubbles as a vehicle for gene and drug delivery: current clinical implications and future perspectives. Current pharmaceutical design 18:2166-2183

35. Dayton PA, Chomas JE, Lum AF, Allen JS, Lindner JR, Simon SI, Ferrara KW (2001) Optical and acoustical dynamics of microbubble contrast agents inside neutrophils. Biophysical journal 80:1547-1556

36. Lindner JR, Coggins MP, Kaul S, Klibanov AL, Brandenburger GH, Ley K (2000) Microbubble persistence in the microcirculation during ischemia/reperfusion and inflammation is caused by integrin- and complement-mediated adherence to activated leukocytes. Circulation 101:668-675

37. Chiou WF, Huang YL, Liu YW (2014) (+)-Vitisin A inhibits osteoclast differentiation by preventing TRAF6 ubiquitination and TRAF6-TAK1 formation to suppress NFATc1 activation. PloS one 9:e89159

38. Irwin R, LaPres JJ, Kinser S, McCabe LR (2007) Prolyl-hydroxylase inhibition and HIF activation in osteoblasts promotes an adipocytic phenotype. Journal of cellular biochemistry 100:762-772

39. Arnett TR, Gibbons DC, Utting JC, Orriss IR, Hoebertz A, Rosendaal M, Meghji S (2003) Hypoxia is a major stimulator of osteoclast formation and bone resorption. Journal of cellular physiology 196:2-8

40. Hamilton JA, Lacey DC, Turner A, de Kok B, Huynh J, Scholz GM (2012) Hypoxia enhances the proliferative response of macrophages to CSF-1 and their pro-survival response to TNF. PloS one 7:e45853

41. Hsieh CP, Chiou YL, Lin CY (2010) Hyperbaric oxygen-stimulated proliferation and growth of osteoblasts may be mediated through the FGF-2/MEK/ERK 1/2/NF-kappaB and PKC/JNK pathways. Connective tissue research 51:497-509

42. Zahm AM, Bucaro MA, Srinivas V, Shapiro IM, Adams CS (2008) Oxygen tension regulates preosteocyte maturation and mineralization. Bone 43:25-31

43. Tuncay OC, Ho D, Barker MK (1994) Oxygen tension regulates osteoblast function. American journal of orthodontics and dentofacial orthopedics : official publication of the American Association of Orthodontists, its constituent societies, and the American Board of Orthodontics 105:457-463

Figure Legends

Figure 1. (a) Ultra-fine bubble aerator (BUVITAS; Ligaric Company Limited, Osaka, Japan). Fine microbubbles of gas were generated after brief sonication. Then UFB were generated using this gas-liquid mixing system with hydrodynamic function. In this apparatus, gas was supplied at 0.1 MPa and 0.7 L/min into microbubble water for 30 min. The high-speed centrifugal force caused by the circulation separates the microbubbles into ultra-fine bubble by the strong shearing force in the dispersed water. (b) Dissolved oxygen concentrations of OUB and NUB diluted saline or medium were measured at 30 minutes after generation by Winkler's method. ††$p<0.01$ vs. non-UFB saline, §$p<0.05$ vs. non-UFB medium. (c) Experimental protocols. All data are expressed by the mean ± SD.

GIO: glucocorticoid-induced osteoporosis, NUB: nitrogen ultra-fine bubbles, OUB: oxygen ultra-fine bubbles, PSL: prednisolone, UFB: ultra-fine bubbles.

Figure 2. (a) Representative micro-CT images of distal femurs in each group (Control, GIO, GIO+OUB and GIO+NUB). (b) Quantitation of trabecular bone parameters (BV/TV and TbN). **p<0.01, *p<0.05. GIO vs. Control, GIO+OUB and GIO+NUB. (c) Quantitation of cortical bone parameters (Cv/Av and Mean cortical bone thickness). *p<0.05. GIO vs. Control, GIO+OUB and GIO+NUB. (d) Representative TRAP-staining in the distal femur of trabecular and cortical bone in each group (Control, GIO, GIO+OUB and GIO+NUB) (200×). (e) The number of TRAP-positive cells per unit trabecular surface were counted using a microscope. **p<0.01 GIO vs. Control, GIO+OUB and GIO+NUB. (f) Serum levels of CTX-1 and osteocalcin in control, GIO and GIO+OUB mice assessed by ELISA. *p<0.05 GIO vs. Control and GIO+OUB. All data are expressed by the mean ± SD.

BV/TV: bone volume fraction (bone volume/total volume), Cv/Av: cortical bone ratio (cortical volume / all volume), CTX-1: cross linked C terminal telopeptides of type I collagen, GIO: glucocorticoid-induced osteoporosis, NUB: nitrogen ultra-fine bubbles, OUB: oxygen ultra-fine bubbles, TbN: trabecular number, TRAP: tartrate resistant acid phosphatase.

Figure 3. Osteoclastic cells were incubated under 20% O_2 condition using mouse BM cells cultured in OUB medium (concentration: 0, 25, 50, 75 and 100%). (a) TRAP-staining was assayed and the number of TRAP-positive cells were counted (200×). *p<0.05 vs. 0%. (b) The bone resorption activity of osteoclasts was assayed using an Osteo-assay plate (200×). *p<0.05 vs.0%. (c) Western blotting of the osteoclasts differentiation-related signals was analyzed. (d) Changes in gene expression for TRAF6, c-Fos, NFATc1, TRAP, Cathepsin K, DC-STAMP, RANK and HIF1α were examined. **p<0.01, *p<0.05 vs. 0%. All data are expressed by the mean ± SD.

BM: bone marrow, ERK: extracellular signal-regulated kinase, DC-STAMP: dendritic cell-specific transmembrane protein, HIF1α: hypoxia-inducible factor 1α, HPRT1: hypoxanthine phosphoribosyltransferase 1, NF-κB: nuclear factor-kappa B, NFATc1: nuclear factor of activated T-cells 1, OUB: oxygen ultra-fine bubble, RANK: receptor activator of nuclear factor kappa B, TRAF6: tumor necrosis factor receptor associated factor 6, TRAP: tartrate resistant acid phosphatase.

Figure 4. Osteoclastic cells were incubated under 5% O_2 condition using mouse BM cells cultured in OUB medium (concentration: 0, 25, 50, 75 and 100%). (a) TRAP-staining was assayed and the number of TRAP-positive cells were counted (200×). *p<0.05 vs. 0%. (b)

Western blotting of HIF1α with whole cell extracts obtained from osteoclasts under normoxic (20% O_2) or hypoxic (5% O_2) conditions in normal medium or OUB diluted medium. (c) Changes in gene expression for TRAF6, c-Fos, NFATc1, TRAP, Cathepsin K, DC-STAMP and HIF1α were examined. *p<0.05 vs. 0%. All data are expressed by the mean ± SD.

BM: bone marrow, DC-STAMP: dendritic cell-specific transmembrane protein, HIF1α: hypoxia-inducible factor 1α, HPRT1: hypoxanthine phosphoribosyltransferase 1, NFATc1: nuclear factor of activated T-cells 1, OUB: oxygen ultra-fine bubble, TRAF6: tumor necrosis factor receptor associated factor 6, TRAP: tartrate resistant acid phosphatase.

Figure 5. (a) Induction of osteoclasts from human PBMC cultured in OUB diluted medium (concentration: 0, 25, 50, 75 and 100%) under 20% O_2 condition and assayed by TRAP-staining (200×). **p<0.01, *p<0.05 vs. 0%. (b) Bone resorption activity of osteoclasts from human PBMC cultured in OUB diluted medium (concentration: 0, 25, 50, 75 and 100%) under 20% O_2 condition and assayed using an Osteo-Assay Plate (200×). **p<0.01, *p<0.05 vs.0%. (c) Schematic representation of the signaling pathways involved in osteoclasts differentiation treated with OUB diluted medium. All data are expressed by the mean ± SD.

AP-1: activator protein 1, DC-STAMP: dendritic cell-specific transmembrane protein, ERK: extracellular signal-regulated kinase, HIF1α: hypoxia-inducible factor 1α, JNK: c-Jun-N-terminal kinase, M-CSF: macrophage colony-stimulating factor, MEK: mitogen-activated protein kinase/ ERK kinase, MKK: mitogen-activated protein kinase kinase, NFATc1: nuclear factor of activated T-cells 1, NF-κB: nuclear factor-kappa B, OUB: oxygen ultra-fine bubble, PBMC: peripheral blood mononuclear cells, RANK: receptor activator of nuclear factor kappa B, RANKL: receptor activator of nuclear factor kappa B ligand, TRAF6: tumor necrosis factor receptor-associated factor 6, TRAP: tartrate-resistant acid phosphatase.

Figure 6. Osteoblastic cells were incubated under 20% O_2 condition. (a) ALP activity and ALP staining were assayed using mouse calvarial cells and MC3T3-E1 cells cultured in OUB diluted medium (concentration: 0, 25, 50, 75 and 100%). (b) Changes in gene expression for ALP, osteocalcin, RANKL, OPG and HIF1α were examined using mouse calvarial cells cultured in OUB diluted medium (concentration: 0, 25, 50, 75 and 100%). All data are expressed by the mean ± SD.

ALP: alkaline phosphatase, HIF1α: hypoxia-inducible factor 1α, HPRT1: hypoxanthine phosphoribosyltransferase 1, OPG: osteoprotegerin, OUB: oxygen ultra-fine bubble, RANKL: receptor activator of nuclear factor kappa B ligand.

Figure

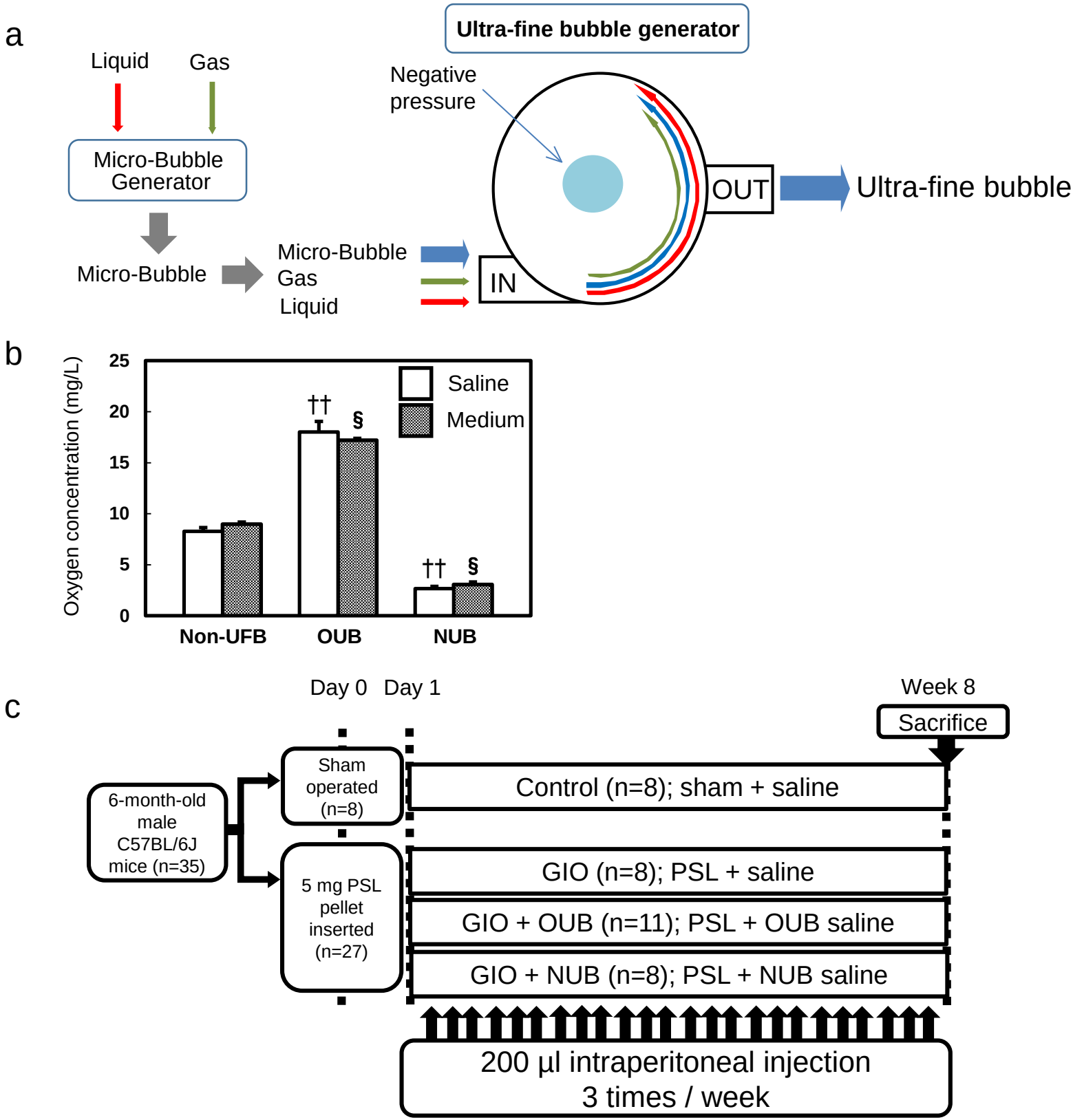
a
Liquid
Gas
Micro-Bubble Generator
Micro-Bubble
Micro-Bubble
Gas
Liquid
Ultra-fine bubble generator
Negative pressure
IN
OUT
Ultra-fine bubble
b
Oxygen concentration (mg/L)
25
20
15
10
5
0
Saline
Medium
††
§
††
§
Non-UFB
OUB
NUB
c
Day 0
Day 1
Week 8
Sacrifice
6-month-old male C57BL/6J mice (n=35)
Sham operated (n=8)
5 mg PSL pellet inserted (n=27)
Control (n=8); sham + saline
GIO (n=8); PSL + saline
GIO + OUB (n=11); PSL + OUB saline
GIO + NUB (n=8); PSL + NUB saline
200 µl intraperitoneal injection
3 times / week

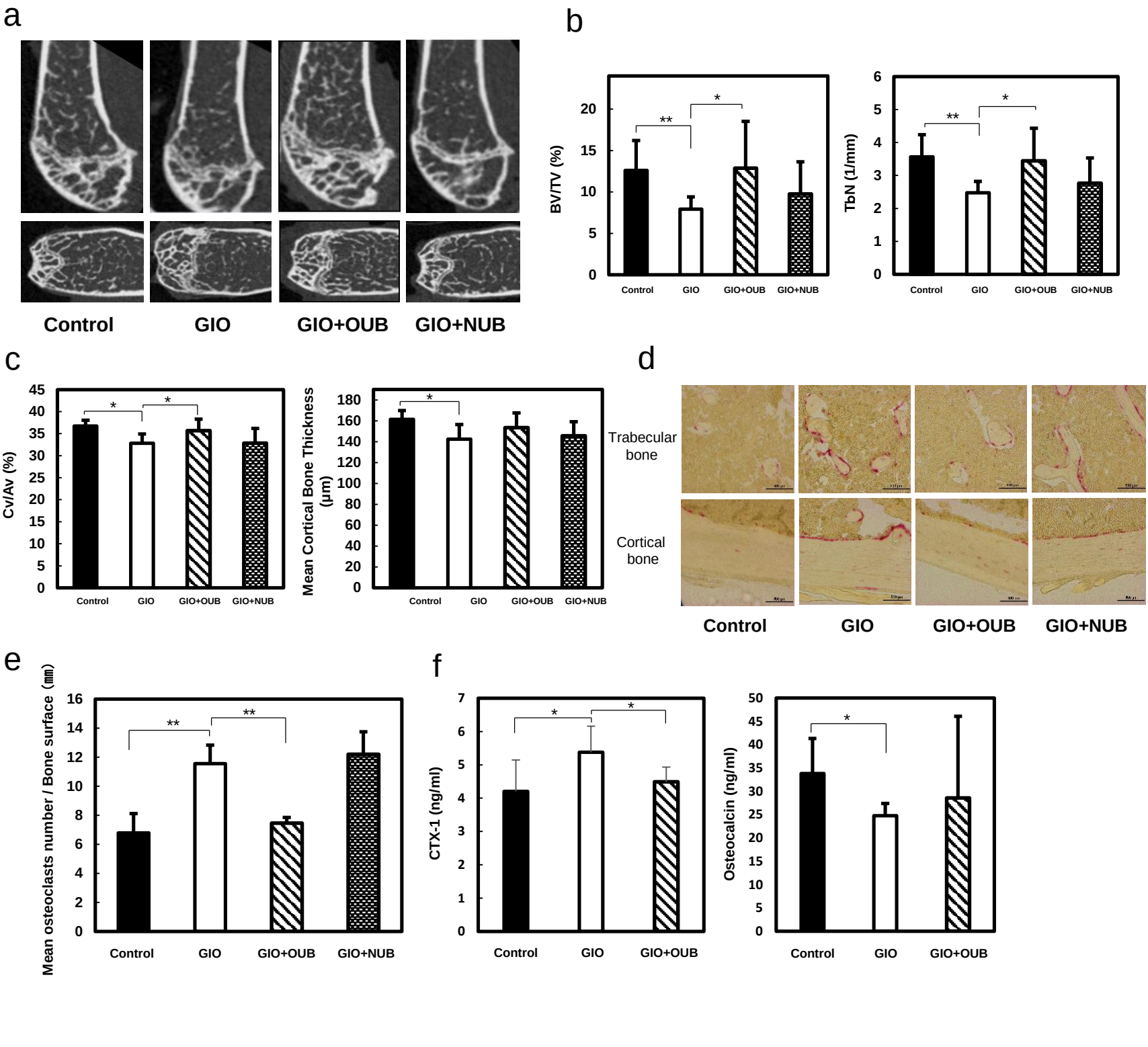
a
Control
GIO
GIO+OUB
GIO+NUB
b
BV/TV (%)
TbN (1/mm)
c
Cv/Av (%)
Mean Cortical Bone Thickness (μm)
d
Trabecular bone
Cortical bone
e
Mean osteoclasts number / Bone surface (㎜)
f
CTX-1 (ng/ml)
Osteocalcin (ng/ml)

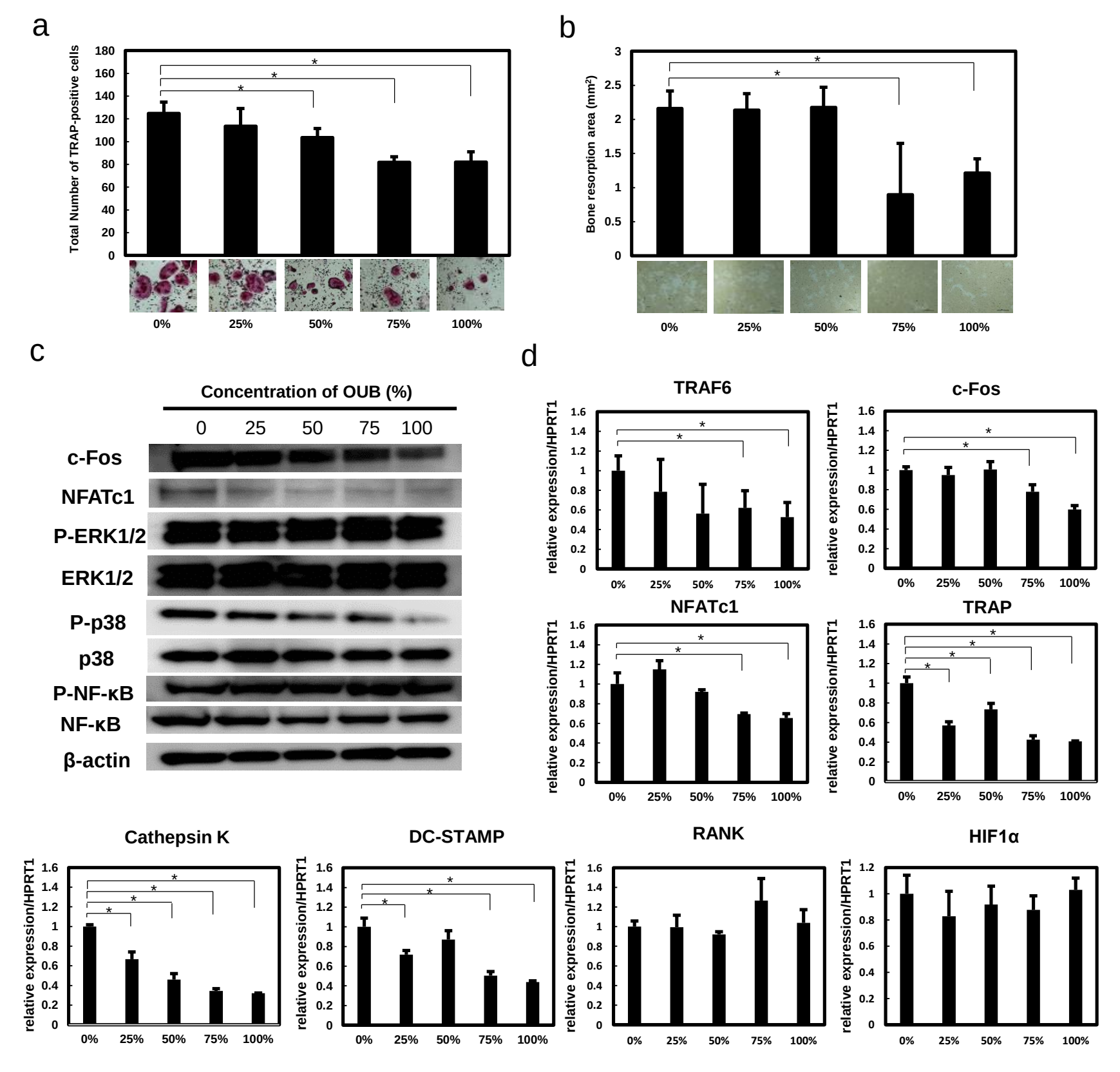
a
Total Number of TRAP-positive cells
180
160
140
120
100
80
60
40
20
0
*
*
*
0%
25%
50%
75%
100%
b
Bone resorption area (mm²)
3
2.5
2
1.5
1
0.5
0
*
*
0%
25%
50%
75%
100%
c
Concentration of OUB (%)
0
25
50
75
100
c-Fos
NFATc1
P-ERK1/2
ERK1/2
P-p38
p38
P-NF-κB
NF-κB
β-actin
d
TRAF6
c-Fos
NFATc1
TRAP
Cathepsin K
DC-STAMP
RANK
HIF1α
relative expression/HPRT1
1.6
1.4
1.2
1
0.8
0.6
0.4
0.2
0
*
0%
25%
50%
75%
100%

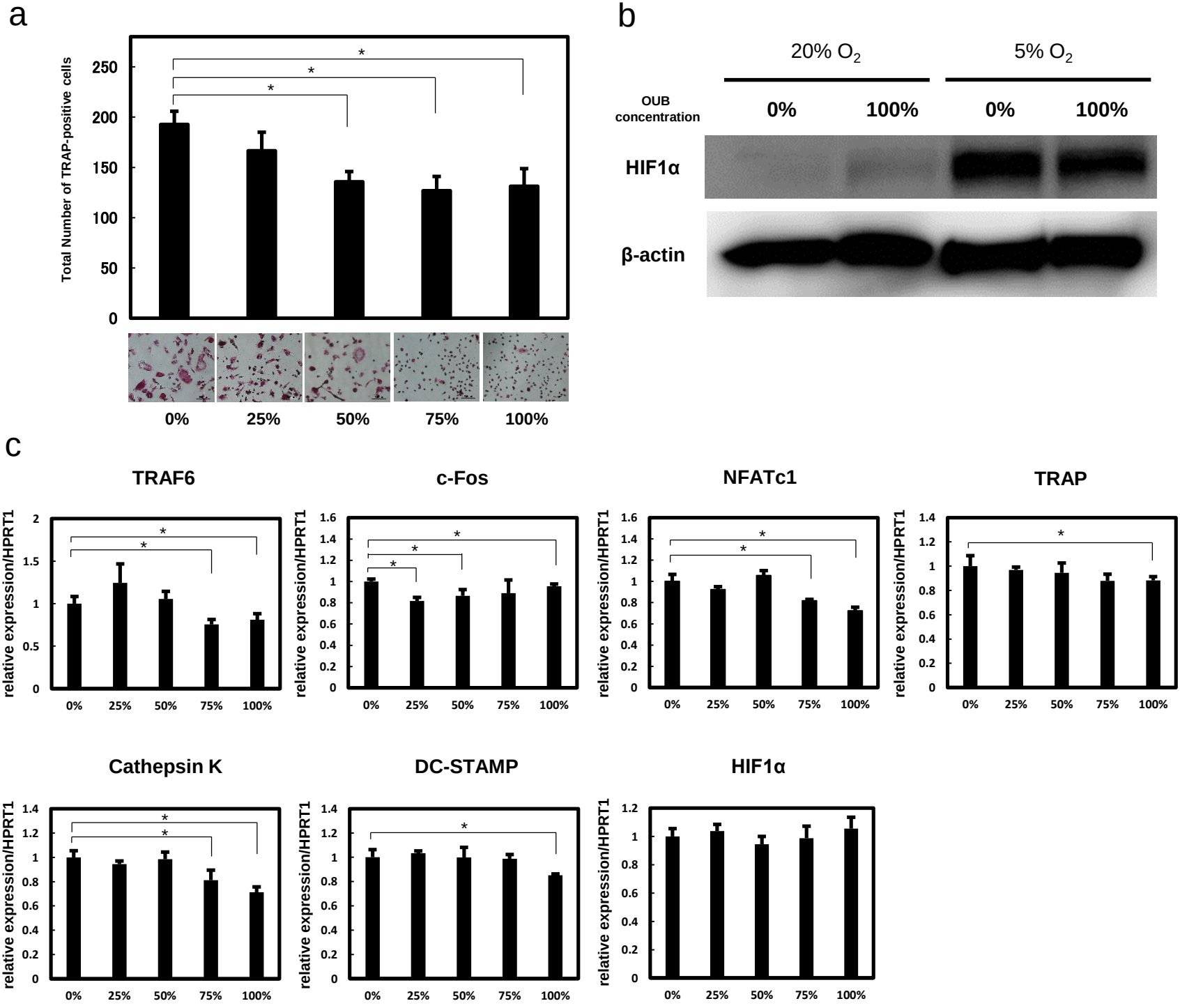
a
Total Number of TRAP-positive cells
250
200
150
100
50
0
*
*
*
0%
25%
50%
75%
100%
b
20% O2
5% O2
OUB concentration
0%
100%
0%
100%
HIF1α
β-actin
c
TRAF6
c-Fos
NFATc1
TRAP
Cathepsin K
DC-STAMP
HIF1α
relative expression/HPRT1
0%
25%
50%
75%
100%

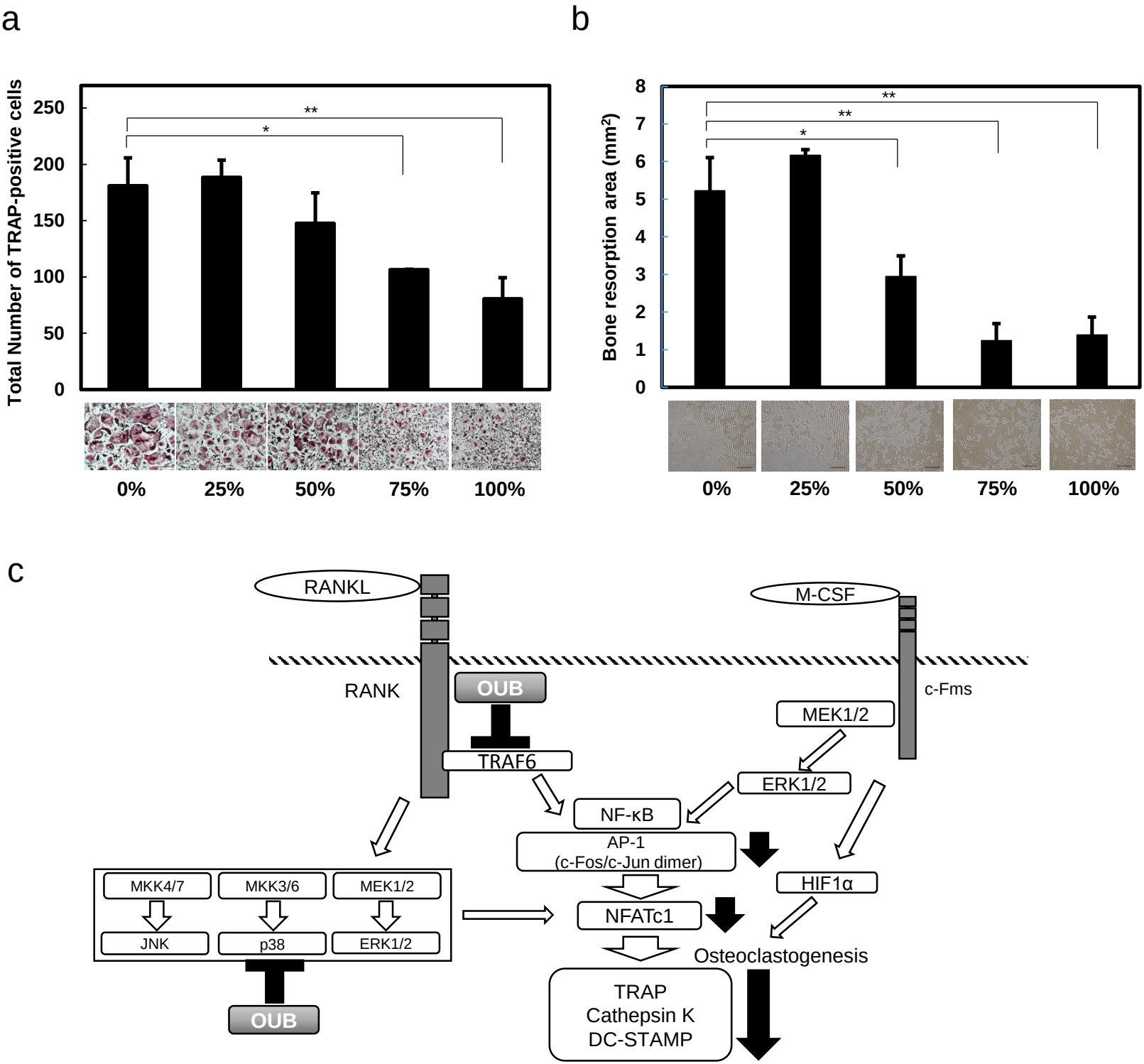
a
Total Number of TRAP-positive cells
250
200
150
100
50
0
**
*
0%
25%
50%
75%
100%
b
Bone resorption area (mm²)
8
7
6
5
4
3
2
1
0
**
**
*
0%
25%
50%
75%
100%
c
RANKL
M-CSF
RANK
OUB
c-Fms
MEK1/2
TRAF6
ERK1/2
NF-κB
AP-1
(c-Fos/c-Jun dimer)
HIF1α
MKK4/7
MKK3/6
MEK1/2
JNK
p38
ERK1/2
NFATc1
Osteoclastogenesis
OUB
TRAP
Cathepsin K
DC-STAMP

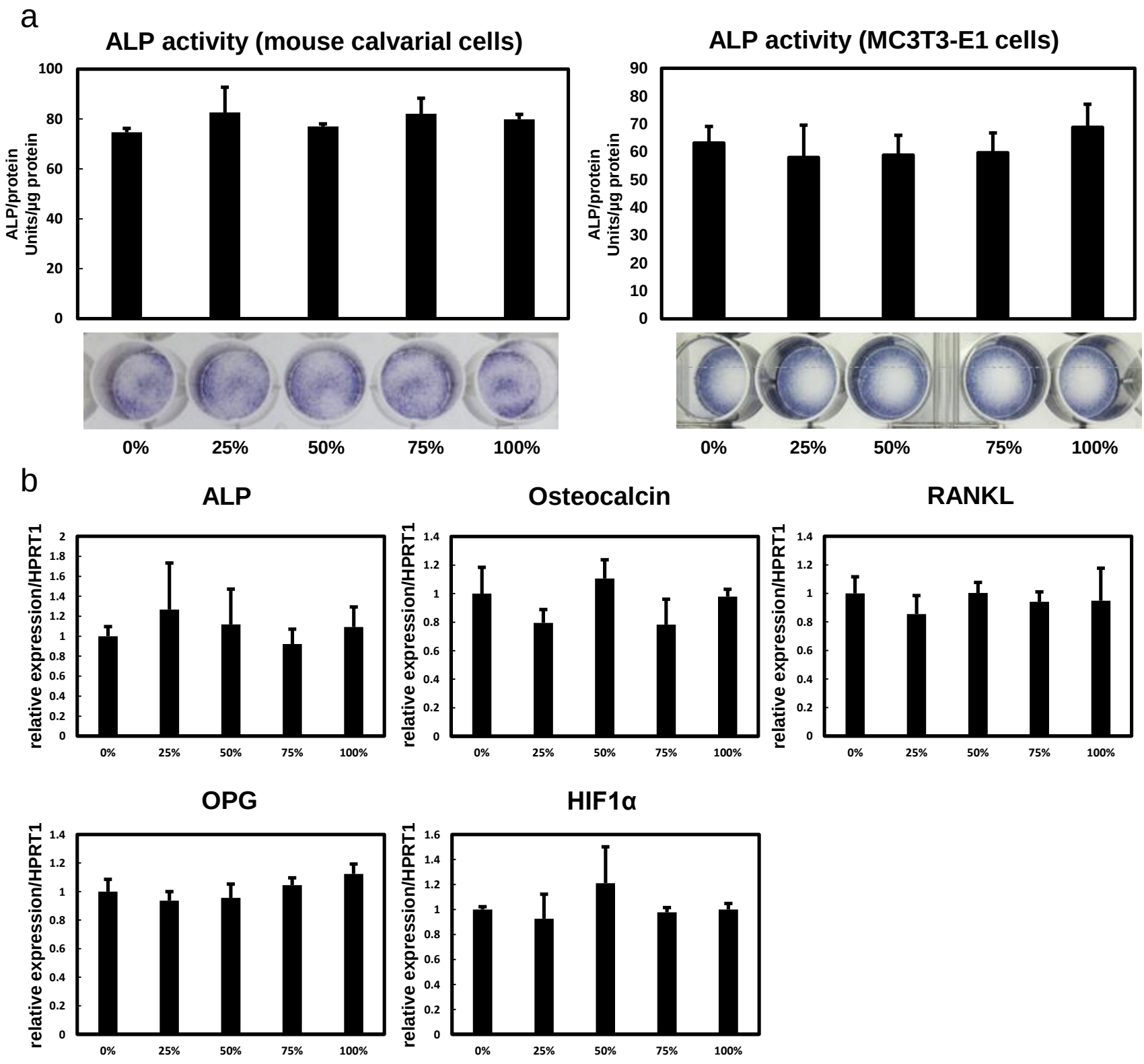
a
ALP activity (mouse calvarial cells)
ALP/protein Units/μg protein
0
20
40
60
80
100
0%
25%
50%
75%
100%
ALP activity (MC3T3-E1 cells)
ALP/protein Units/μg protein
0
10
20
30
40
50
60
70
80
90
0%
25%
50%
75%
100%
b
ALP
relative expression/HPRT1
0
0.2
0.4
0.6
0.8
1
1.2
1.4
1.6
1.8
2
0%
25%
50%
75%
100%
Osteocalcin
relative expression/HPRT1
0
0.2
0.4
0.6
0.8
1
1.2
1.4
0%
25%
50%
75%
100%
RANKL
relative expression/HPRT1
0
0.2
0.4
0.6
0.8
1
1.2
1.4
0%
25%
50%
75%
100%
OPG
relative expression/HPRT1
0
0.2
0.4
0.6
0.8
1
1.2
1.4
0%
25%
50%
75%
100%
HIF1α
relative expression/HPRT1
0
0.2
0.4
0.6
0.8
1
1.2
1.4
1.6
0%
25%
50%
75%
100%

Supplemental data

Original Article

Oxygen ultra-fine bubbles water administration prevents bone loss of glucocorticoid-induced osteoporosis in mice by suppressing osteoclasts differentiation

Takaaki Noguchi, MD[a], Kosuke Ebina, MD, PhD[a]*, Makoto Hirao, MD, PhD[a], Tokimitsu Morimoto, MD, PhD[a], Kota Koizumi, MD, PhD[a], Kazuma Kitaguchi, MD[a], Hozo Matsuoka, MD[a], Toru Iwahashi, MD[a], Hideki Yoshikawa, MD, PhD[a]

[a] *Department of Orthopaedic Surgery, Osaka University, Graduate School of Medicine, 2-2 Yamadaoka, Suita, Osaka 565-0871, Japan*

*Corresponding author:

Phone: +81 6 6879 3552; FAX: +81 6 6879 3559

E-mail address: k-ebina@umin.ac.jp (K. Ebina)

Supplemental Materials and methods

Seven-week-old male C57BL/6J mice were purchased from Charles River Laboratories (Osaka, Japan), and 200 µl of saline or OUB diluted saline (which were filtered with 220 nm pore size cellulose acetate membrane to avoid contamination) was intraperitoneally injected in 5 mice for each group. Five minutes after the injection, serum was collected, heparinized, and filtered, then kept in 4°C with the tight lid. The next day (24hr later), concentration and size (10-2000 nm) of nanoparticles of both group serum (×10,000 diluted) were measured by NanoSight NS 300 (NanoSight Ltd, Salisbury, UK) as previously described [2]. Filtered normal saline (negative control) and filtered OUB diluted saline (positive control) were measured at the same time.

Chemical analysis of metal nanoparticles in both raw water and air UFB diluted water was performed by using NexION 350D ICP-MS spectrometer (PerkinElmer Inc., Shelton, USA).

Supplemental Figure 1.

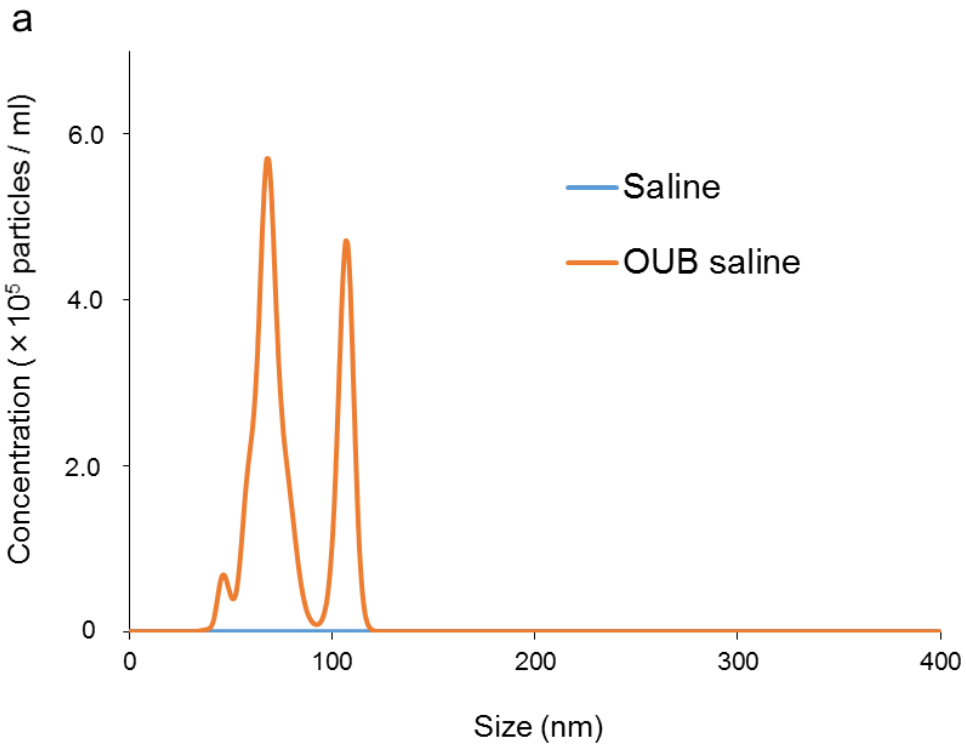

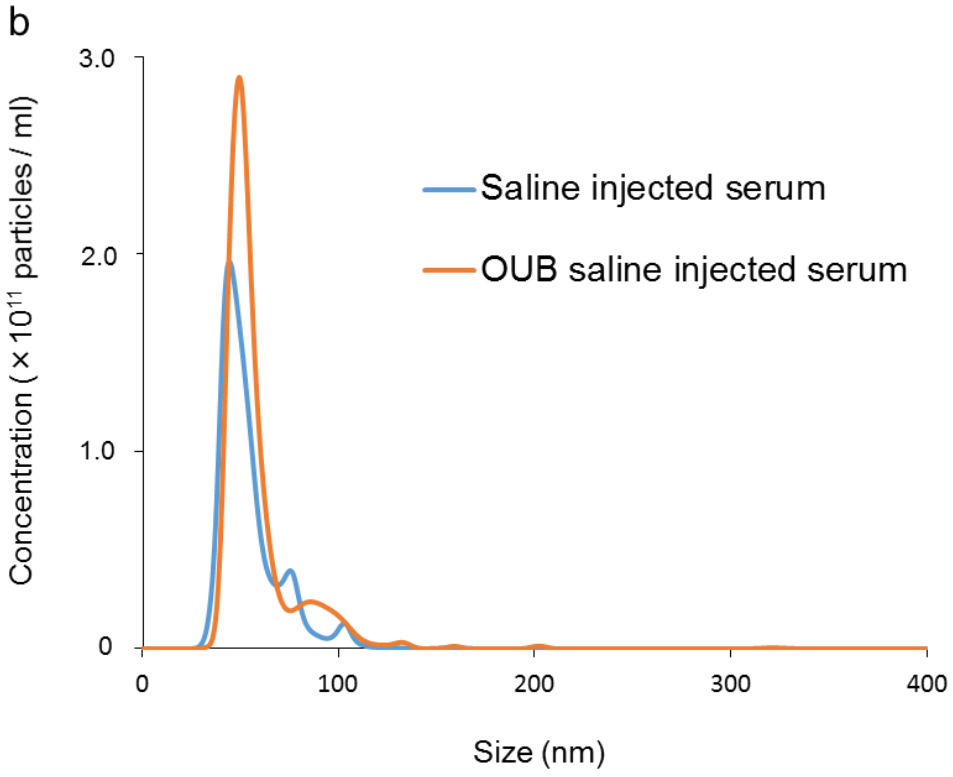

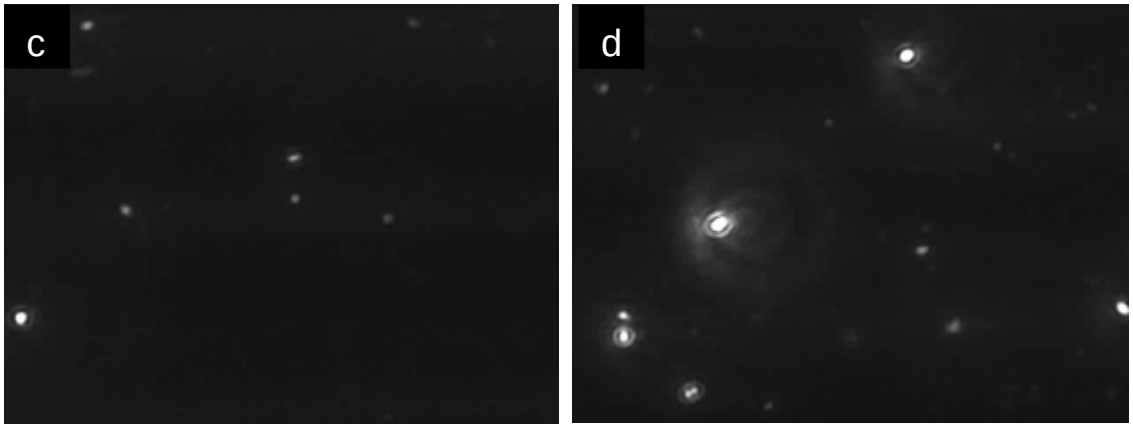

Supplemental Figure 1. Comparison of the nanoparticles concentration and size distribution between saline and OUB diluted saline (a), and saline injected mice serum (n=5) and OUB saline injected mice serum (n=5) (b). Visualization of nanoparticles' Brownian motion in saline injected mice serum (c) and OUB saline injected mice serum (d).

Serum samples were ×10,000 diluted, and all the samples were filtered with 220 nm pore size cellulose acetate membrane to avoid contamination.

Supplemental Figure 2.

	Li (μg/L)	Be (μg/L)	B (μg/L)	Na (μg/L)	Mg (μg/L)	Al (μg/L)	K-1 (μg/L)	Ca-1 (μg/L)	Sc-1 (μg/L)	Ti (μg/L)	V-1 (μg/L)	Cr-1 (μg/L)
Raw water	0.00	0.00	-0.67	24.20	0.93	-0.02	2.25	14.46	-0.01	-0.04	0.00	0.00
Air UFB water	0.01	0.00	-1.05	18.29	0.73	-0.07	2.24	12.20	-0.01	-0.06	0.00	0.00
	Mn (μg/L)	Fe-2 (μg/L)	Co (μg/L)	Ni (μg/L)	Cu (μg/L)	Zn-1 (μg/L)	Ga (μg/L)	Ge (μg/L)	As (μg/L)	Se-1 (μg/L)	Rb (μg/L)	Sr (μg/L)
Raw water	-0.01	-0.16	0.00	0.00	-0.05	0.29	0.00	0.01	-0.20	-0.13	0.00	0.02
Air UFB water	-0.01	-0.18	0.00	0.01	-0.07	0.30	0.00	0.00	-0.10	-0.25	0.00	0.01
	Y (μg/L)	Zr (μg/L)	Nb (μg/L)	Mo (μg/L)	Ru (μg/L)	Rh (μg/L)	Pd (μg/L)	Ag (μg/L)	Cd (μg/L)	Sn (μg/L)	Sb (μg/L)	Te (μg/L)
Raw water	0.00	0.00	0.00	0.00	0.00	-0.41	0.00	0.00	0.00	0.01	0.01	0.01
Air UFB water	0.00	0.00	0.00	0.00	0.00	-0.54	0.00	0.00	0.00	0.01	0.01	0.01
	Cs (μg/L)	Ba (μg/L)	La (μg/L)	Hf (μg/L)	Ta (μg/L)	W (μg/L)	Re (μg/L)	Ir (μg/L)	Pt (μg/L)	Au (μg/L)	Tl (μg/L)	Pb (μg/L)
Raw water	0.00	0.00	0.00	0.00	0.00	0.00	0.00	0.00	0.00	0.00	0.00	0.00
Air UFB water	0.00	0.00	0.00	0.00	0.00	0.00	0.00	0.01	0.00	0.00	0.00	0.00
	Bi (μg/L)	Ce (μg/L)	Pr (μg/L)	Nd (μg/L)	Sm (μg/L)	Eu (μg/L)	Gd (μg/L)	Tb (μg/L)	Dy (μg/L)	Ho (μg/L)	Er (μg/L)	Tm (μg/L)
Raw water	0.00	0.00	0.00	0.00	0.00	0.00	0.00	0.00	0.00	0.00	0.00	0.00
Air UFB water	0.00	0.00	0.00	0.00	0.00	0.00	0.00	0.00	0.00	0.00	0.00	0.00
	Yb (μg/L)	Lu (μg/L)	Th (μg/L)	U (μg/L)	Mg (μg/L)							
Raw water	0.00	0.00	0.00	0.00	0.00							
Air UFB water	0.00	0.00	0.00	0.00	0.00							

Supplemental Figure 2. Concentration of metal nanoparticles in both raw water and air-UFB water.